

## SUPPLEMENTARY MATERIAL

1. PETROGRAPHIC DESCRIPTION OF ANALYZED SAMPLES
  2. DETAILS ON THE ANALYTICAL METHODS
  3. DETAILS ON SAMPLE BOR14-2
  4. COMPOSITION OF THE BASEMENT OF THE WESTERN GHATS
  5. MAJOR ELEMENT MODELLING
  6. CHOICE OF MODELLING SOFTWARE AND THERMAL AND CHEMICAL PARAMETERS FOR THE EC-AFC MODELLING
- FIGURE S1: TAS CLASSIFICATION DIAGRAM
  - FIGURE S2: THIN SECTION IMAGES
  - FIGURE S3: MAJOR ELEMENT VARIATIONS
  - FIGURE S4: MAJOR ELEMENT VS ISOTOPIC RATIO VARIATIONS
  - FIGURE S5: ISOTOPIC COMPOSITIONS OF BASEMENT ROCKS
  - FIGURE S6: VARIABLE CRUSTAL COMPOSITIONS AND TEMPERATURES IN ASSIMILATION MODELLING
  - FIGURE S7: MCS ASSIMILATION MODELLING OF SR-ND ISOTOPIC VARIATIONS STARTING FROM A A HIGH-TI PICRITE (NORTHERN DECCAN) AND A HIGH-MG HIGH-TI BASALT
  - FIGURE S8 EC-AFC MODELLING OF ISOTOPIC VARIATIONS STARTING FROM A RÈUNION BASALT AND FROM A HIGH-TI PICRITE (NORTHERN DECCAN)
  - FIGURE S9: TRACE ELEMENT VARIATIONS, MCS AND EC-AFC ASSIMILATION MODELLING
  - TABLE S1: EXCEL FILE WITH COMPLETE WHOLE-ROCK DATA SET
  - TABLE S2, S3: EXCEL FILES WITH PARAMETERS USED FOR CRUSTAL ASSIMILATION MCS AND EC-AFC MODELLING.

## *1S. PETROGRAPHIC DESCRIPTION OF ANALYZED SAMPLES*

The analysed rock samples are tholeiitic basalts (total-alkali-silica classification in Figure S1) collected from the central, massive (i.e., vesicle-free) portion of lava flows from the Western Ghats (thin section images in Figure S2). These are holocrystalline, porphyritic rocks, generally with an isotropic texture (apart from local alignments of plagioclase tablets defining a magmatic flow). The analysed rock samples are characterized by the occurrence of phenocrysts (along with glomerophyric crystal aggregates) in a microcrystalline groundmass. Phenocrysts mainly consist of plagioclase, clinopyroxene (mostly augite and marginally pigeonite), minor orthopyroxene and rare olivine, which is only exceptionally preserved. The modal proportion of phenocrysts ranges between ca. 5% and 15%. Ambenali samples are those with lowest proportions of phenocrysts. Glomerophyric crystal aggregates, up to 5 mm, generally contain plagioclase and clinopyroxene in different proportions, with clot-forming crystals up to 1 mm (Capriolo et al., 2024). The microcrystalline groundmass consists of the same mineral components plus Fe–Ti oxides, specifically ilmenite and magnetite in equal proportions. Hydrothermal alteration and weathering are generally minor, and selectively affect specific mineral phases, in particular olivine (systematically replaced by fine-grained aggregates of iddingsite) and occasionally plagioclase (rarely affected by partial sericitization). Sample BOR14-2 shows coarser grain sizes, higher percentage of phenocrysts, and slightly different mineral composition compared to the other samples, and is thus considered as a cumulate. Glomerophyric crystal aggregates are generally dominated by clinopyroxene (modal content exceeding 60%) while altered olivine is interstitial along the rims of these clinopyroxene clots. Similar cumulate rocks are well known from the Thakurvadi formation (Shekhar et al., 2024). Because of relatively abundant altered olivine in sample BOR14-2, its LOI is higher than that of other rock samples, without any further petrographic evidence for deeper or more pervasive hydrothermal alteration and weathering.

## 2S. DETAILED ANALYTICAL METHODS

All samples were crushed to fine powders in an agate mill. Low W contents ( $< 1$  ppm and comparable or lower than the BCR2 standard) indicate that chalcophile and siderophile elements were not contaminated by handling in the laboratory. Loss on ignition is the weight loss after heating the sample to 110 and 1000 °C for 24 hours (LOI 110 °C and LOI 1000 in Tables S1, LOI tot being the sum of the two).

Whole-rock major element and selected trace element contents were determined by X-ray fluorescence (XRF) at the University of Padova with a Philips PW2400 spectrometer (procedures in Boscaini et al. (2022). Major element totals are calculated on a dry basis. Trace elements were also analysed by Inductively Coupled Plasma–Mass Spectrometry (ICP-MS) at the University of Bretagne Occidentale at Brest (France), following analytical protocols described in Barrat et al. (1996).

Radiogenic isotope ratios of Sr ( $^{87}\text{Sr}/^{86}\text{Sr}$ ), Nd ( $^{143}\text{Nd}/^{144}\text{Nd}$ ) and Pb ( $^{206}\text{Pb}/^{204}\text{Pb}$ ,  $^{207}\text{Pb}/^{204}\text{Pb}$ ,  $^{208}\text{Pb}/^{204}\text{Pb}$ ) were measured at the Department of Earth Sciences (University of Geneva, Switzerland). Between 100 and 120 mg of whole rock powder were dissolved during 7 days in Savillex® Teflon vials using 4 ml of concentrated HF and 1 ml of HNO<sub>3</sub> 14M, at a temperature of 140 °C and with the help of ultrasonication for 30 minutes twice a day. Subsequently, samples were dried and re-dissolved for 3 days (also with 30 minutes ultrasonication twice a day) in 3 ml of HNO<sub>3</sub> 14M and dried again. Sr, Nd and Pb were then separated using cascade columns with Sr-Spec, TRU-Spec and Ln-Spec resins according to a protocol modified from Pin et al. (1994). Finally, the material was redissolved in 2% HNO<sub>3</sub> solutions and ratios were measured using a Thermo Neptune PLUS Multi-Collector ICP-MS in static mode. Ratios used to monitor internal fractionation were:  $^{88}\text{Sr}/^{86}\text{Sr} = 8.375209$  for the  $^{87}\text{Sr}/^{86}\text{Sr}$  ratio,  $^{146}\text{Nd}/^{144}\text{Nd} = 0.7219$  for the  $^{143}\text{Nd}/^{144}\text{Nd}$  ratio and  $^{203}\text{Tl}/^{205}\text{Tl} = 0.418922$  for the three Pb ratios (a Tl standard was added to the solution). Used external standards were SRM987 ( $^{87}\text{Sr}/^{86}\text{Sr} = 0.710248$ ; McArthur et al., 2001; long-term external reproducibility: 17 ppm, 1SD), JNdi-1 ( $^{143}\text{Nd}/^{144}\text{Nd} = 0.512115$ ; Tanaka et al.,

2000; long-term external reproducibility: 14 ppm, 1SD), and SRM981 (Baker et al., 2004) for Pb (long-term 1SD external reproducibility of 0.0083% for  $^{206}\text{Pb}/^{204}\text{Pb}$ , 0.0071% for  $^{207}\text{Pb}/^{204}\text{Pb}$  and 0.0095% for  $^{208}\text{Pb}/^{204}\text{Pb}$ ).  $^{87}\text{Sr}/^{86}\text{Sr}$ ,  $^{143}\text{Nd}/^{144}\text{Nd}$  and Pb isotope ratios were further corrected for external fractionation (due to systematic differences between measured and accepted standard ratios) by values of -0.021‰, +0.051‰ and +0.36‰ amu respectively. Interferences at masses 84 ( $^{84}\text{Kr}$ ), 86 ( $^{86}\text{Kr}$ ) and 87 ( $^{87}\text{Rb}$ ) were corrected by monitoring  $^{83}\text{Kr}$  and  $^{85}\text{Rb}$ ,  $^{144}\text{Sm}$  interference on  $^{144}\text{Nd}$  was monitored on the mass  $^{147}\text{Sm}$  and corrected by using a  $^{144}\text{Sm}/^{147}\text{Sm}$  value of 0.206700 and  $^{204}\text{Hg}$  interference on  $^{204}\text{Pb}$  was corrected by monitoring  $^{202}\text{Hg}$ . Total procedural blanks were <500 pg for Pb and <100 pg for Sr and Nd which are insignificant compared to the amounts of these elements purified from the whole rock samples investigated.

Re-Os Analytical Techniques. Approximately 1 gram of whole-rock sample powder, 2 mL of double-distilled concentrated HCl, 5 mL of double-distilled concentrated  $\text{HNO}_3$ , purged by  $\text{N}_2$  bubbling to remove  $\text{OsO}_4$  impurities, and appropriate amounts of a mixed  $^{185}\text{Re}$  -  $^{190}\text{Os}$  enriched isotopic tracer solution (spike) were sealed in quartz vessels and heated in a high-pressure asher (Anton-Paar HPA) to 260 °C for 16 hours. Osmium was extracted twice from the acid solution using liquid  $\text{Br}_2$ , then back-extracted into HBr added to the liquid  $\text{Br}_2$  and further purified by microdistillation, using techniques adapted from those of Birck et al. (1997) and Nakanishi et al. (2019). Rhenium was separated and from the residual acidic solution with  $\text{HNO}_3$  using columns filled with anion exchange resin (AG1-X8, 200-400 mesh).

Osmium isotope ratios were measured as  $\text{OsO}_3^-$  by negative thermal ionization mass spectrometry (N-TIMS; Creaser et al., 1991; Völkening et al., 1991) using either a Finnigan MAT262 or a ThermoScientific Triton instrument at the CRPG laboratory. All samples were measured using a secondary electron multiplier in peak-jumping mode. The measured isotopic ratios were corrected for mass fractionation assuming  $^{192}\text{Os}/^{188}\text{Os} = 3.08271$  (Nier, 1937), using an off-line routine that iteratively corrects for fractionation, heavy oxide isobaric interferences, and the spike contribution. Rhenium isotopic ratios used for isotope dilution calculations were measured using an MC-ICPMS

instrument (ThermoScientific Neptune). These measurements were performed using a secondary electron multiplier in peak-jumping mode, with isotopic mass fractionation corrected by interspersal of samples with Re liquid standards.

Total mean procedural blanks associated with this project were  $0.84 \pm 0.94$  pg with  $^{187}\text{Os}/^{188}\text{Os} = 0.22 \pm 0.11$  ( $2s$ ;  $n=4$ ) for Os and  $7.8 \pm 3.9$  pg ( $2s$ ;  $n=5$ ) for Re. All data shown in Table 1 have been corrected for the blank contributions. Re-Os uncertainties in Table 1 are  $2\sigma$  values and include all identified sources of uncertainty (in-run analytical precision,  $2s$  isotopic variability of in-house liquid standard,  $2s$  variability of blank amount and isotopic composition, potential contribution of isobaric interference of  $^{187}\text{ReO}_3$  on  $^{187}\text{OsO}_3$ ). Two analyses of the peridotite reference material UB-N yielded, respectively,  $^{187}\text{Os}/^{188}\text{Os} = 0.12714$  and  $0.12718$ ;  $[\text{Os}] = 3.99$  and  $3.54$  ppb;  $[\text{Re}] = 0.215$  and  $0.224$  ppb.

### 3S. DETAILS ON SAMPLE BOR14-2

Among the samples analyzed here, BOR14-2 is anomalous because of its coarse-grained, cumulate texture, which suggests that its whole-rock composition cannot be considered as representative of a magmatic liquid. Moreover, BOR14-2 has a relatively high LOI (2.84 wt.%) possibly due to post-magmatic alteration. Other studies (e.g., Beane et al., 1986; Melluso et al., 2004; Chatterjee, 2024; Shekhar et al., 2024) have documented the presence of high-MgO Thakurvadi samples (Fig. S3), which are usually considered as olivine or clinopyroxene cumulates.

Notably, anomalously radiogenic Os isotopic compositions were found also by Peters et al. (2017) for coarse-grained samples with  $> 3.00$  wt.% LOI. BOR14-2 has the highest  $^{187}\text{Os}/^{188}\text{Os}_i$  (0.211) of our samples but nevertheless plots within the initial ratio range (0.117 to 0.62) from literature data for the Deccan and overlaps with Os isotopic compositions of samples with high LOI ( $> 3$  wt.%) (Peters et al., 2017; Peters and Day (2017). BOR14-2 also has extreme very high  $^{87}\text{Sr}/^{86}\text{Sr}$  (0.70978) and low  $^{143}\text{Nd}/^{144}\text{Nd}$  (0.51191) and Pb ( $^{206}\text{Pb}/^{204}\text{Pb} = 17.28$ ) initial isotopic compositions, which

would suggest high degrees of crustal assimilation. However, the match between the calculated (with EC-AFC) and the observed isotopic composition is poor for this sample and its high MgO content (13.5 wt.%) seems inconsistent with the calculated amounts of assimilation and fractionation (ca. 30 wt.%). Therefore, the highly radiogenic Sr-Pb-Os isotopic compositions of sample BOR14-2 may at least in part be explained by post- or syn-magmatic alteration as suggested also by Peters and Day (2017) for some of their Deccan samples. However, alteration alone does not explain the low  $^{143}\text{Nd}/^{144}\text{Nd}_i$  (0.51191), suggesting that crustal assimilation may have contributed to the composition of this rock.

#### *4S. COMPOSITION OF THE WESTERN GHATS BASEMENT*

South of the WG, the Dharwar craton is divided into two main blocks, the West and the East Dharwar. Most rocks from the West and East Dharwar range in age from ca. 3.4 to ca. 2.5 Ga and are mainly felsic intrusives and metamorphic (gneissic) rocks (Manykiamba et al., 2024). Dykes of felsic to mafic composition are present in the craton and range in age from 2.4 to 1.8 Ga. Published Sr-Nd-Pb isotopic data for the Dharwar felsic and mafic rocks are not very abundant, but show a very large range of compositions (Fig. S5). Sr-Nd-Pb isotopic were recalculated to 66 Ma. These values recalculated to 66 Ma are generally enriched, for example Nd isotopic compositions range from 0.5120 to 0.5105. Pb isotopic compositions also show a very large range, e.g., ca. 14 to 25 for  $^{206}\text{Pb}/^{204}\text{Pb}$ .

North of the WG, in the Central India Tectonic Zone, dominantly felsic Lower to Mid-Proterozoic crustal rocks show a large range of compositions resulting from melting of Archean to Early Proterozoic crustal rocks (e.g., Mishra et al., 2024; Yousouf et al., 2019). Their published  $^{87}\text{Sr}/^{86}\text{Sr}$  and  $^{143}\text{Nd}/^{144}\text{Nd}$  compositions range from 0.720 to 0.830 and from 0.5118 to 0.5112, respectively. A thin sedimentary cover of Late Paleozoic to Early Mesozoic age is locally present in the Narmada-Tapi grabens. The sediments are mainly continental siliciclastic rocks composed of reworked Proterozoic felsic rocks.

Late Proterozoic basement rocks (ca. 0.7-0.8 Ga) are known from the Seychelles (Ashwal et al., 2002; Shellnutt et al., 2020) and possibly extended to the basement of the NW Deccan (e.g., the Saurashtra Peninsula; Ashwal et al., 2013).  $^{87}\text{Sr}/^{86}\text{Sr}$  and  $^{143}\text{Nd}/^{144}\text{Nd}$  compositions for Seychelles and NW Deccan basement range from 0.712 to 1.2 and from 0.5125 to 0.5120, respectively, for granitoids, from 0.705 to 0.712 and from 0.5127 to 0.5123 for intermediate and mafic rocks (Ashwal et al., 2002).

Crustal xenoliths have been found in a few dykes from the Deccan tholeiites and associated alkaline rocks (e.g., Dessai et al., 2004; Ray et al., 2008). Crustal xenoliths in the Murud lamprophyre (near the Arabian Sea coast) are mafic to ultramafic (no isotopic values have been published), while those from tholeiitic Deccan dykes in the Satpura Range (North of the WG) are mainly Si-rich metamorphic rocks. Ray et al. (2008) obtained  $^{87}\text{Sr}/^{86}\text{Sr}$  on the felsic metamorphic rocks (0.714 to 0.780) and, based on the isotopic and major and trace element data, concluded that the crustal xenoliths are similar to Dharwar craton rocks. The presence of Dharwar rocks underneath the Deccan flows is supported by data from the Koyna drill-core in the southern part of the WG (Khanna et al., 2024). Basement rocks at Koyna are arc-related basaltic to silicic rocks of Archean age (ca. 2.5 Ga), which resemble those from the Western Dharwar craton.

In summary, the most likely basement rocks directly under the WG are Archean in age and belong to the Dharwar craton. Proterozoic basement rocks (mainly Mid Proterozoic in age) outcrop to the North of the WG and may not have present in the area of the Main Deccan studied here.

## *5S. MODELLING OF OPEN SYSTEM MAJOR ELEMENT VARIATIONS*

Major element variations have been modelled using the Magma Chamber Simulator (MCS) code (Bohrson et al., 2020). We used MCS to model assimilation of partial melts of the wall-rocks, rather than bulk-rock assimilation (note that the latter process, stoping, can be modelled with MCS via the recharge function). The starting compositions considered here are a high-Ti basalt (JEB15) from the Thakurvadi Fm. (Basu et al., 2020), and a high-Ti and a low-Ti picrite (or picritic basalt) from the

northern Deccan (D44 and D56; Melluso et al., 2006). Considered crustal assimilates in the modelling are a granite from the Dharwar craton (Ravindran et al., 2019) and a granulite (as calculated by Taylor and McLennan, 1985; whole-rock composition and temperature, e.g., solidus, data are reported in Table S2 and results are shown in Fig. S3).

Compositions with MgO similar to those of the studied basalts are reached after 45-55 wt.% fractionation. In general, the overlap between modelled and observed compositions is not very good, supporting the conclusion that several distinct parental magma compositions are required in order to reproduce the large range of WG basalt compositions. Liquid lines of descent (LLD) calculated for picrites from the Northern Deccan (low and high-Ti picrites) generally fail to reproduce the observed compositions of WG basalts. Slightly better results are obtained for high-Ti WG basalts (from the Wai Subgroup, in particular) starting from a high-Ti and high-Mg Thakurvadi basalt as parental magma. In general, the overlap between modelled and observed K<sub>2</sub>O contents is poor. This may suggest either that this element is affected by post-magmatic mobilization or that the considered parental rocks are too K<sub>2</sub>O rich.

For a relatively low initial temperature of the wall-rock (400 °C), the solidus of the selected granitic assimilant (calculated to be ca. 660 °C by MCS modelling) is reached (i.e., crustal melts start to be produced) after more than 50 wt.% crystallization of the primary basalt. In contrast, for a higher initial wall-rock temperature of 600 °C (i.e., closer to the solidus), crustal melting and assimilation would start after about 10 wt.% crystallization of the primary magma. Figure S3 g-h shows that in the case of the “cold” granite, the maximum amount of assimilation is about 3 wt.% for the resulting magmas to still maintain a basaltic composition (SiO<sub>2</sub> < 52 wt.%, MgO 2-4 wt.%). On the contrary, for the “hot” granite case, the maximum amount of assimilation would be ca. 9 wt.%, resulting in SiO<sub>2</sub> and MgO contents higher than 52 and 3 wt.%, respectively, in which case the resulting magma would be more evolved than most analyzed WG basalts.

Assimilation of a lower crustal granulite (initial T 650 °C and assumed solidus T ca. 700 °C) would start after ca. 10-15 wt.% crystallization of the primary basalt. Compared to close-system



differentiation (e.g., Marzoli et al., 2022), the calculated major element composition of the contaminated magma is not strongly modified by the granulite assimilation even for as much as 30 wt.% assimilation. We note that similar results were obtained by Heinonen et al. (2021). The MCS code was also used to model trace element and isotopic ratio variations. The results are shown in the Supplementary Information Figures S7, S9c. The calculated compositions overlap only a small part of the observed compositions.

## *6S. CHOICE OF SOFTWARE, THERMAL AND GEOCHEMICAL PARAMETERS FOR CRUSTAL ASSIMILATION MODELLING*

### *6.1S Choice of MCS vs EC-AFC*

The discrepancy of modelled vs. observed compositions (Fig. S7, S9c) probably suggests that the considered primitive melt compositions cannot be parental magmas of most WG basalts. In fact, according to previous studies (references in the main text), it is well established that basalts from distinct subgroups and possibly from distinct formations require different parental magmas. In particular, it is unlikely that parental magmas of the WG basalts were picrites from the Northern Deccan, which erupted on a different craton, probably at a different age compared to the WG basalts. It is also unlikely that MgO-rich magmatic rocks from the Kalsubai can be parental to Wai Subgroup basalts. In fact, all known near-primitive rocks from the Deccan have isotopic compositions and trace element ratios which are significantly more enriched than Wai Subgroup (and in particular Ambenali Formation) basalts. Therefore, the absence of suitable parental magmatic rocks (in particular for the Wai formations) in the Deccan unfortunately hinders the possibility to properly use the MCS code for modelling the evolution of WG basalts. As a consequence, we preferred to use the simpler EC-AFC code, which requires less assumptions on the parental magma compositions.

Furthermore, the MCS code is not implemented to model sulfide crystallization. As Re and Os contents in evolved magmas and in crustal melts are mainly controlled by sulfide crystallization and

melting, MCS is not the best choice to model Os isotopic variations during open-system crustal contamination processes. In the case of the EC-AFC model, the variation of Os requires the choice of reasonable solid/melt partition coefficients. The choice of these values are discussed below.

#### 6.2S Parental magma compositions.

For the EC-AFC modelling we had to back-calculate trace element compositions, starting from Ambenali basalt compositions and assuming ca. 50% fractionation of olivine and clinopyroxene and plagioclase (in proportions 20, 40, 40%), while the isotopic compositions are those of the analyzed Ambenali basalts. Moreover, we selected the previously cited low and high-Ti picrites from the Northern Deccan plus the high-MgO basalt from the Thakurvadi Formation as possible parental magmas.

#### 6.3S Mineral/basalt partition coefficients

These have been calculated for the relevant trace elements (REE, Sr, Pb, Nb, Th), considering that the main fractionating minerals of the basaltic magmas are plagioclase and clinopyroxene plus less abundant oxides. Indeed, these trace elements are virtually completely incompatible in the other potentially early crystallizing minerals (e.g., olivine, Cr-spinel and subsequently magnetite). The only exception is Nb, which may be only moderately incompatible in Ti-magnetite (Nielsen and Beard, 2000). The partition coefficients for plagioclase are from Aigner Torres et al. (2007), while clinopyroxene D values are from Hill et al. (2000). The plagioclase/clinopyroxene ratio has been considered = 1, and magnetite is assumed to represent 10% of the total amount of fractionated minerals, according to the MELTS modelling done in Marzoli et al. (2022) starting from Kalsubai high-MgO magmatic compositions (SAM011, BOR036; Beane et al., 1986). Os has a compatible behavior in basaltic magmas, as is evidenced also by its correlation with Ni (see main text Fig. 4). In Fig. S6 of this supplementary file we modelled the variation of the  $^{187}\text{Os}/^{188}\text{Os}$  composition of the evolving magma vs. the amount of assimilated crustal mass fraction. Fig. S6a shows the results

for variable partition coefficients for Os, from 10 to 4. As expected, the  $^{187}\text{Os}/^{188}\text{Os}$  of the contaminated magma increases more rapidly at higher  $D_{\text{Os}}$  for a given amount of assimilated crust. For magmas having  $^{187}\text{Os}/^{188}\text{Os}$  lower than 0.17, the mass fraction of assimilated crust is lower than 0.06, regardless of the tested partition coefficient.

#### 6.4S The isotopic compositions of the starting magmas and assimilants.

In the main text figures, we show the EC-AFC curves starting from both the Ambenali-like and the low-Ti picrite composition. Magma compositions have been assumed to be equal to those of the Ambenali basalts studied here and of a low-Ti picrite from Melluso et al. (2006). The  $^{187}\text{Os}/^{188}\text{Os}$  of the low-Ti picrite is from the low-Ti picrites studied by Peters et al. (2017). Fig. S6b shows the  $^{187}\text{Os}/^{188}\text{Os}$  vs assimilated mass fraction starting from the Ambenali and low-Ti picrite.

The initial Os content of the parental magma has been considered as 300 ppt, corresponding to the Os contents of typical primitive continental basalts (Carlson, 2005). The highest Os contents in Peters et al. (2017) are ca. 600 ppt. For such high Os content in the parental magma a slightly larger amount of crustal assimilation would be required to reach a given  $^{187}\text{Os}/^{188}\text{Os}$  in the contaminated magma (e.g., ca. 7.3% vs ca. 3.6% for 600 and 300 ppt Os to reach  $^{187}\text{Os}/^{188}\text{Os} = 0.15$  in the contaminated magma; Fig. S6c).

The most critical parameter for the EC-AFC models is the isotopic composition of the assimilant. For Sr-Nd-Pb isotopic ratios, a relatively large number of data are available in the literature for the Dharwar craton and the Proterozoic terranes north of the WG (see previous section). We have considered two felsic contaminants, with the values reported in Table S2. The selected isotopic compositions plot at the extremes of the Sr-Pb isotopic data range plotted in Fig. S5. To our knowledge, no data have been published for the Os isotopic composition of Indian Proterozoic to Archean crustal rocks, therefore we used calculated values. We can approximately calculate the  $^{187}\text{Os}/^{188}\text{Os}$  of the crust, considering typical Re and Os contents of the continental crust (Esser and Turekian, 1993; Saal et al., 1999; Peucker Ehrenbring and Jahn, 2001; Carlson, 2005). Considering

the age of the potential basement rocks, we tested a range of  $^{187}\text{Os}/^{188}\text{Os}$  from 0.8 to 1.5 for the felsic crust (values consistent with the age of the basement rocks) starting from an Ambenali (dashed lines) and from a low-Ti picrite (continuous line; Fig. S6b). The estimated  $^{187}\text{Os}/^{188}\text{Os}$  values for felsic Dharwar rocks are consistent with data reported by Peucker-Ehrenbrink and Jahn (2001) for the average felsic continental crust. Obviously, the  $^{187}\text{Os}/^{188}\text{Os}$  of the contaminated magma increases more rapidly when the assimilant has a high  $^{187}\text{Os}/^{188}\text{Os}$  value ( $\geq 1.2$ ), likely typical of Lower Proterozoic to Archean basement crust. However, even when the assimilant has a relatively low  $^{187}\text{Os}/^{188}\text{Os}$  ratio (e.g., 0.8), incorporating about 10% crust is still sufficient to raise the magma  $^{187}\text{Os}/^{188}\text{Os}$  above 0.17.

The Os content of the assimilant also exerts a strong control on the composition of the contaminated magma. In the EC-AFC models starting from Ambenali parental magma and shown in the main text, we used a fairly conservative value of 30 ppt for the felsic crust, equal to the estimated average composition of the upper crust (ca. 30 ppt; Rudnick and Gao, 2014). For the EC-AFC models starting from the low-Ti picrite, the Os content of the felsic crust is assumed to be 15 ppt. This value is at the low end of the range of Os contents reported for felsic rocks (Peucker-Ehrenbrink and Jahn, 2001, and references therein).

We also tested the assimilation of mafic granulites. Re and Os contents (Table S3) are taken from Saal et al. (1998), considering both average and extreme values (e.g., granulite 1 and 2 in Fig S6f) and  $^{187}\text{Os}/^{188}\text{Os}$  calculated for ages of 2.5, 2.0, and 1.0 Ga. For all considered granulite compositions, the  $^{187}\text{Os}/^{188}\text{Os}$  of the calculated magma rapidly increases to more than 0.20 with less than 1% assimilation.

Finally, modelling of a Réunion basalt as parental magma are shown in Fig. S7. The assimilated felsic crustal rocks are the same as those reported in Table S2. The general results are not significantly different from those considering the Ambenali basalt as parental magma.

#### 6.5S The initial T of the magma and of the crust

The initial T of the magma has been assumed as 1300 °C for the EC-AFC results shown in the figures of the main text. This T is consistent with the liquidus T calculated with MELTS for high-MgO Kalsubai magmas (Marzoli et al., 2022). At higher T, the Os content of the crystallizing magma decreases rapidly before the assimilation starts and then the calculated  $^{187}\text{Os}/^{188}\text{Os}$  of the contaminated magma increases relatively rapidly at low fractions of assimilated crust, but would still be lower than ca. 0.16 for <10% assimilated mass (Fig. S6d).

Finally, we tested assimilation models for the initial temperature of the felsic crust ranging from 300 to 550 °C (Fig. S5d). The former T corresponds to a typical T of the crust (not affected by recent magmatic intrusions) at ca. 10 km depth, while 550 °C is equivalent to the assumed solidus T of the felsic crust in the EC-AFC models (note that the same exercise has been done with MCS, but with a calculated solidus T of 660 °C and initial T at 400 and 600 °C slightly higher than those used for EC-AFC modelling, see section 5S). At low crustal T, a significant amount of crystallization is required before the crust reaches the solidus. Therefore, the assimilation process is delayed and only starts when the magma is already evolved and has attained low Os concentrations. At higher crustal T, the assimilation starts sooner and the  $^{187}\text{Os}/^{188}\text{Os}$  of the magma increases concurrently. Therefore, for a low and high crustal T the amounts of assimilation of the contaminated magma to achieve  $^{187}\text{Os}/^{188}\text{Os} = 0.17$  are ca. 4% and 6%, respectively.

In summary, it can reasonably be concluded that  $^{187}\text{Os}/^{188}\text{Os}$  compositions <0.15 in basalts allow for only very limited amounts of crustal contamination, most probably less than 8% for the felsic crust and less than 1% for a mafic granulite.

## References

- Aigner-Torres, M., Blundy, J., Ulmer, P., Pettke, T., 2007. Laser ablation ICPMS study of trace element partitioning between plagioclase and basaltic melts: an experimental approach. *Contributions to Mineralogy and Petrology* 153, 647–667, <https://doi.org/10.1007/s00410-006-0168-2>.

- Alam, M., Mishra, M.K., Kaulina, T.V., Ahmad, T., Choudhary, A.K., 2022. Geochemistry and petrogenesis of Proterozoic granitoids from Central Indian Tectonic Zone (CITZ): elemental and isotopic constraints. *Geochem. J.* 56, 160–176.
- Ashwal, L.D., Demaiffe, D., Torsvik, T.H., 2002. Petrogenesis of Neoproterozoic granitoids and related rocks from the Seychelles: the case for an Andean-type arc origin. *J. Petrol.* 43, 45–83.
- Ashwal, L.D., Solanki, A.M., Pandit, M.K., Corfu, F., Hendriks, B.W.H., Burke, K., Torsvik, T.H., 2013. Geochronology and geochemistry of Neoproterozoic Mt. Abu granitoids, NW India: regional correlation and implications for Rodinia paleogeography. *Precamb. Res.* 236, 265–281.
- Baker, J., Peate, D., Waight, T., Meyzen C., 2004. Pb isotopic analysis of standards and samples using a  $^{207}\text{Pb}$ - $^{204}\text{Pb}$  double spike and thallium to correct for mass bias with a double-focusing MC-ICPMS. *Chem. Geol.* 211, 275–303.
- Barrat, J. A., Keller, F., Amossé, J., Taylor, R. N., Nesbitt, R. W., Hirata, T., 1996. Determination of rare earth elements in sixteen silicate reference samples by ICP-MS after TM addition and ion exchange separation. *Geostandards and Geoanalytical Research* 20, 133–139.
- Basu, A.R., Saha-yannopoulos, A., Chakrabarty, P., 2020. Lithos A precise geochemical volcano-stratigraphy of the Deccan traps. *Lithos* 376–377, 105754.  
<https://doi.org/10.1016/j.lithos.2020.105754>
- Beane, J.E., Turner, C.A., Hooper, P.R., Subbarao, K. V, Walsh, J.N., 1986. Stratigraphy, composition and form of the Deccan Basalts, Western Ghats, India. *Bull. Volcanol.* 48, 61–83.  
<https://doi.org/10.1007/BF01073513>
- Birck J.-L. Roy Barman M. & Capmas F., 1997. Re-Os isotopic measurements at the femtomole level in natural samples. *Geostandards Newsletter. The Journal of Geostandards and Geoanalysis* 21, 19–27.

- Bohrson, W. A., Spera, F. J., Heinonen, J. S., Brown, G. A., Scruggs, M. A., Adams, J. V., Takach, M. K., Zeff, G., and Suikkanen, E., 2020. Diagnosing open-system magmatic processes using the Magma Chamber Simulator (MCS): part I—major elements and phase equilibria. *Contrib. Mineral. Petrol.* 175, 1-29.
- Carlson, R.W., 2005. Application of the Pt–Re–Os isotopic systems to mantle geochemistry and geochronology. *Lithos* 82, 249–272. doi.org/10.1016/j.lithos.2004.08.003
- Chatterjee, N., 2024. Petrogenesis of the Deccan high-Mg basalts and picrites. *Contrib. Mineral. Petrol.* 179, 90, <https://doi.org/10.1007/s00410-024-02172-7>
- Chiaradia, M., Müntener, O., Beate, B., 2020. Effects of aseismic ridge subduction on the geochemistry of frontal arc magmas. *Earth Planet. Sci. Letters* 531, 115984, <https://doi.org/10.1016/j.epsl.2019.115984>.
- Creaser, R.A., Papanastassiou, D.A., Wasserburg, G.J., 1991. Negative thermal ion mass spectrometry of osmium, rhenium and iridium. *Geochim. Cosmochim. Acta* 55, 397–401. [https://doi.org/10.1016/0016-7037\(91\)90427-7](https://doi.org/10.1016/0016-7037(91)90427-7)
- Dessai, A.G., Markwick, A., Vaselli, O., Downes, H., 2004. Granulite and pyroxenite xenoliths from the Deccan Trap: insight into the nature and composition of the lower lithosphere beneath cratonic India. *Lithos* 78, 263-290, doi.org/10.1016/j.lithos.2004.04.038.
- Halfar, M.C., Peters, B.J., Day, J.M.D., Schönbächler, M., 2023. An isotopically enriched mantle component in the source of Rodrigues, Réunion volcanic hotspot. *Geochim. Cosmochim. Acta* 355, 32–47. <https://doi.org/10.1016/j.gca.2023.06.030>
- Heinonen, J. S., Spera, F. J., Bohrson, W. A., 2021. Thermodynamic limits for assimilation of silicate crust in primitive magmas. *Geology* 50, 81–85, <https://doi.org/10.1130/G49139.1>

- Hill, E., Wood, B.J., Blundy, J.D., 2000. The effect of Ca-Tschermaks component on trace element partitioning between clinopyroxene and silicate melt. *Lithos* 53, 203–215.
- Le Bas, M. J., Le Maitre, R. W., Streckeisen, A. & Zanettin, B., 1986. A chemical classification of volcanic rocks based on the total alkali-silica diagram. *Journal of Petrology* 27, 745–750.
- Khanna, T. C., Barbeau, D. L., 2024. Zircon U-Pb geochronology and geochemistry of hot subduction volcanic suite in the deep bore-hole well-core KBH-5: Evidence of Neoproterozoic Shimoga greenstone belt beneath the Cretaceous Deccan Traps, India. *Lithos* 482–483, 107692, <https://doi.org/10.1016/j.lithos.2024.107692>
- Manikyamba, C., Upadhyay, D., Mohan, M. R., 2024. Archean crustal evolution and craton formation in peninsular India: new insights from the Singhbhum, Dharwar and Bastar Cratons. *Proc. Indian Natl. Sci. Acad.* 90, 167–195 <https://doi.org/10.1007/s43538-024-00254-5>
- Marzoli, A., Renne, P.R., Andreasen, R., Spiess, R., Chiaradia, M., Ruth, D.C.S., Tholt, A.J., Pande, K., Costa, F., 2022. The Shallow Magmatic Plumbing System of the Deccan Traps, Evidence from Plagioclase Megacrysts and Their Host Lavas. *J. Petrol.* 63, 1–32. <https://doi.org/10.1093/petrology/egac075>
- McArthur, J.M., Howarth, R. J., Bailey, T. R., 2001. Strontium Isotope Stratigraphy: LOWESS Version 3: Best Fit to the Marine Sr-Isotope Curve for 0–509 Ma and Accompanying Look-up Table for Deriving Numerical Age. *The J. of Geol.* 109, 155–170.
- Melluso, L., Sethna, S.F., D’Antonio, M., Javeri, P., Bennio, L., 2002. Geochemistry and petrogenesis of sodic and potassic mafic alkaline rocks in the Deccan Volcanic Province, Mumbai Area (India). *Mineral. Petrol.* 74, 323–342, [doi.org/10.1007/s007100200009](https://doi.org/10.1007/s007100200009)



- Melluso, L., Barbieri, M., Beccaluva, L., 2004. Chemical evolution, petrogenesis, and regional chemical correlations of the flood basalt sequence in the central Deccan Traps, India. *J. Earth Syst Sci* 113, 587–603. <https://doi.org/10.1007/BF02704024>
- Melluso, L., Mahoney, J.J., Dallai, L., 2006. Mantle sources and crustal input as recorded in high-Mg Deccan Traps basalts of Gujarat (India). *Lithos* 89, 259-274, [doi.org/10.1016/j.lithos.2005.12.007](https://doi.org/10.1016/j.lithos.2005.12.007).
- Mishra, M.K., Alam, M., Kaulina, T.V. et al. 2024. Geochemical characterization and zircon U–Pb geochronology of the Tirodi Gneissic Complex, Central Indian Tectonic Zone (CITZ): constraints on petrogenesis, Proterozoic crustal evolution and tectonic setting. *Miner Petrol* 118, 159–183. <https://doi.org/10.1007/s00710-024-00853-6>
- Mohan, M.R., McNaughton, N.J., Sarma, D.S., Rajamanickam, M., Fletcher, I.R., Wilde, S.A., Rasmussen, B., Krapež, B., Balakrishnan, S., 2023. Petrogenesis of Meso-Neoproterozoic granitoids from the Chitradurga Greenstone Belt: Implications on crustal growth and reworking of the Dharwar Craton, southern India. *J. Asian Earth Sci.* 242, 105494.
- Nielsen, R.L., Beard, J.S., 2000. Magnetite–melt HFSE partitioning. *Chemical Geology* 164, 21-34, [doi.org/10.1016/S0009-2541\(99\)00139-4](https://doi.org/10.1016/S0009-2541(99)00139-4).
- Pakulla, J.J., Jansen, M.W., Duraiswami, R.A., Gadpallu, P., Tusch, J., Jentsch, C., Braukmüller, N., Wombacher, F., Münker, C., 2023. Trace element and Sr-Nd-Hf-Pb isotope evidence for a multi-magma chamber system beneath the Deccan Volcanic Province, India. *Chem. Geol.* 640, 121749. [doi.org/10.1016/j.chemgeo.2023.121749](https://doi.org/10.1016/j.chemgeo.2023.121749)
- Peters, B.J., Day, J.M.D., 2017. A geochemical link between plume head and tail volcanism. *Geochemical Perspect. Lett.* 5, 29–34. [https://doi.org/https://doi.org/10.7185/geochemlet.1742](https://doi.org/10.7185/geochemlet.1742)

- Peters, B.J., Day, J.M.D., Greenwood, R.C., Hilton, D.R., Gibson, J., Franchi, I.A., 2017. Helium – oxygen – osmium isotopic and elemental constraints on the mantle sources of the Deccan Traps. *Earth Planet. Sci. Lett.* 478, 245–257. <https://doi.org/10.1016/j.epsl.2017.08.042>
- Peucat, J.J., Vidal, P., Bernard-Griffiths J., Condie, K.C., 1989. Sr, Nd, and Pb isotopic systematics in the Archean low- to high-grade transition zone of southern India: syn-accretion vs. post-accretion granulites. *Journal of Geology* 97, 537–550.
- Peucat, J. J., Jayananda, M., Chardon, D., Capdevila, R., Fanning, C. M., Paquette, J-L., 2013. The lower crust of the Dharwar Craton, Southern India: Patchwork of Archean granulitic domains. *Prec. Res.* 227, 4-28, <https://doi.org/10.1016/j.precamres.2012.06.009>.
- Peucker-Ehrenbrink, B., Jahn, B., 2001. Rhenium-osmium isotope systematics and platinum group element concentrations: Loess and the upper continental crust. *Geochemistry, Geophys. Geosystems* 2. <https://doi.org/https://doi.org/10.1029/2001GC000172>
- Pin, C., Briot, D., Bassin, C., & Poitrasson, F., 1994. Concomitant separation of strontium and samarium-neodymium for isotopic analysis in silicate samples, based on specific extraction chromatography. *Analytica Chimica Acta*, 298(2), 209-217.
- Ravindran, A., Mezger, K., Balakrishnan, S., Berndt, J., 2021. Hf-Nd isotopes from ultramafic and mafic rocks in the western Dharwar Craton, India, record early Archean mantle heterogeneity. *Lithos* 404–405, 106491
- Ravindran, A., Mezger, K., Balakrishnan, S., Berndt, J., Ranjan, S., Upadhyay, D., 2023. Formation of Paleo- to Meso-Archean continental crust in the western Dharwar Craton, India: Constraints from U–Pb zircon ages and Hf-Pb-Sr isotopes of granitoids and sedimentary rocks *Chem. Geol.* 615, 121196

- Ravindran, A., Mezger, K., Balakrishnan, S., Kooijman, E., Schmitt, M., Berndt, J., 2020. Initial  $^{87}\text{Sr}/^{86}\text{Sr}$  as a sensitive tracer of archaean crust-mantle evolution: constraints from igneous and sedimentary rocks in the western Dharwar Craton, India. *Precambrian Res.* 337, 105523
- Ray, R., Shukla, A. D., Sheth, H. C., Ray, J. S., Duraiswami, R. A., Vanderkluysen, L., Rautela, Mallik, C. S. J., 2008. Highly heterogeneous Precambrian basement under the central Deccan Traps, India: Direct evidence from xenoliths in dykes. *Gondw. Res.* 13, 375-385, <https://doi.org/10.1016/j.gr.2007.10.005>.
- Rickers, K., Mezger, K., Raith, M. M., 2001. Evolution of the Continental Crust in the Proterozoic Eastern Ghats Belt, India and new constraints for Rodinia reconstruction: implications from Sm–Nd, Rb–Sr and Pb–Pb isotopes. *Precambrian Research* 112, 183-210, [https://doi.org/10.1016/S0301-9268\(01\)00146-2](https://doi.org/10.1016/S0301-9268(01)00146-2).
- Rudnick, R.L., Gao, S., 2014. Composition of the continental crust. In: Holland, H.D. & Turekian, K.K. (eds.) *Treatise on Geochemistry* 3. UK (Oxford): Elsevier, pp. 1–64.
- Saal, A.E., Rudnick, R.L., Ravizza, G.E., Hart, S.R., 1998. Re–Os isotope evidence for the composition, formation and age of the lower continental crust. *Nature* 393, 58.
- Shekhar, A., Jourdan, F., Cucciniello, C., Naik, A., Sheth, H., Astha, B., 2024. Geology and  $^{40}\text{Ar}/^{39}\text{Ar}$  age of the Khopoli olivine gabbro intrusion, Konkan Plain, western Deccan Traps. *Geological Magazine* 161 e12. doi:10.1017/S0016756824000293
- Shellnutt, J. G., Nguyen, D. T., Lee, H-Y., 2020). Resolving the origin of the Seychelles microcontinent: Insight from zircon geochronology and Hf isotopes. *Precambrian Research* 343, 105725, <https://doi.org/10.1016/j.precamres.2020.105725>.
- Shukla, M., Verma, S. K., Malviya, V. P., Oliveira, E. P., S., Umrao, R. K., Prakash, S., Torres, E. E., 2025. Crustal reworking during the transition of tectonic regime in the Paleoproterozoic Era: Constraints from geochemistry, Sm–Nd isotope and U–Pb geochronology of granitic

gneisses, Dudhi Granitoid Complex, Mahakoshal belt, Central Indian Tectonic Zone (CITZ), India. *Precambrian Research* 417, 107660, <https://doi.org/10.1016/j.precamres.2024.107660>.

Simonetti, A., Goldstein, S.L., Schmidberger, S.S., Viladkar, S.G., 1998. Geochemical and Nd, Pb, and Sr Isotope Data from Deccan Alkaline Complexes—Inferences for Mantle Sources and Plume–Lithosphere Interaction. *J. Petrol.* 39, 1847–1864. <https://doi.org/10.1093/petroj/39.11-12.1847>

Sun, S.-S. & McDonough, W. F., 1989. Chemical and isotopic systematics of oceanic basalts: Implications for mantle composition and processes. In: Saunders, A. D. & Norry, M. J. (eds) *Magmatism in the Ocean Basins*. London, UK: Geological Society, London, UK: Special Publications 42, 313–345.

Talukdar, M., Sarkar, T., Sengupta, P., Mukhopadhyay, D., 2022. The Southern Granulite Terrane, India: The saga of over 2 billion years of Earth’s history. *Earth-Science Rev.* 232, 104157. <https://doi.org/https://doi.org/10.1016/j.earscirev.2022.104157>

Tanaka, T., Togashi, S., Kamioka, H., Amakawa, H., Kagami, H., Hamamoto, T., et al., 2000. JNdi-1: a neodymium isotopic reference in consistency with LaJolla neodymium. *Chemical Geol.* 168, 279-281.

Taylor S. R. & McLennan S. M. 1985. *The Continental Crust: Its Composition and Evolution*. xvi + 312 pp. Oxford, London, Edinburgh, Boston, Palo Alto, Melbourne: Blackwell Scientific.

Völkening, J., Walczyk, T., G. Heumann, K., 1991. Osmium isotope ratio determinations by negative thermal ionization mass spectrometry. *Int. J. Mass Spectrom. Ion Process.* 105, 147–159. [doi.org/10.1016/0168-1176\(91\)80077-Z](https://doi.org/10.1016/0168-1176(91)80077-Z)

Yousuf, I., Subba Rao, D. V., Balakrishnan, S., Ahmad, T., 2019. Geochemistry and petrogenesis of acidic volcanics from Betul–Chhindwara Belt, Central Indian Tectonic Zone (CITZ), central India. *Journal of Earth System Science* 128, 8, <https://doi.org/10.1007/s12040-019-1255-x>

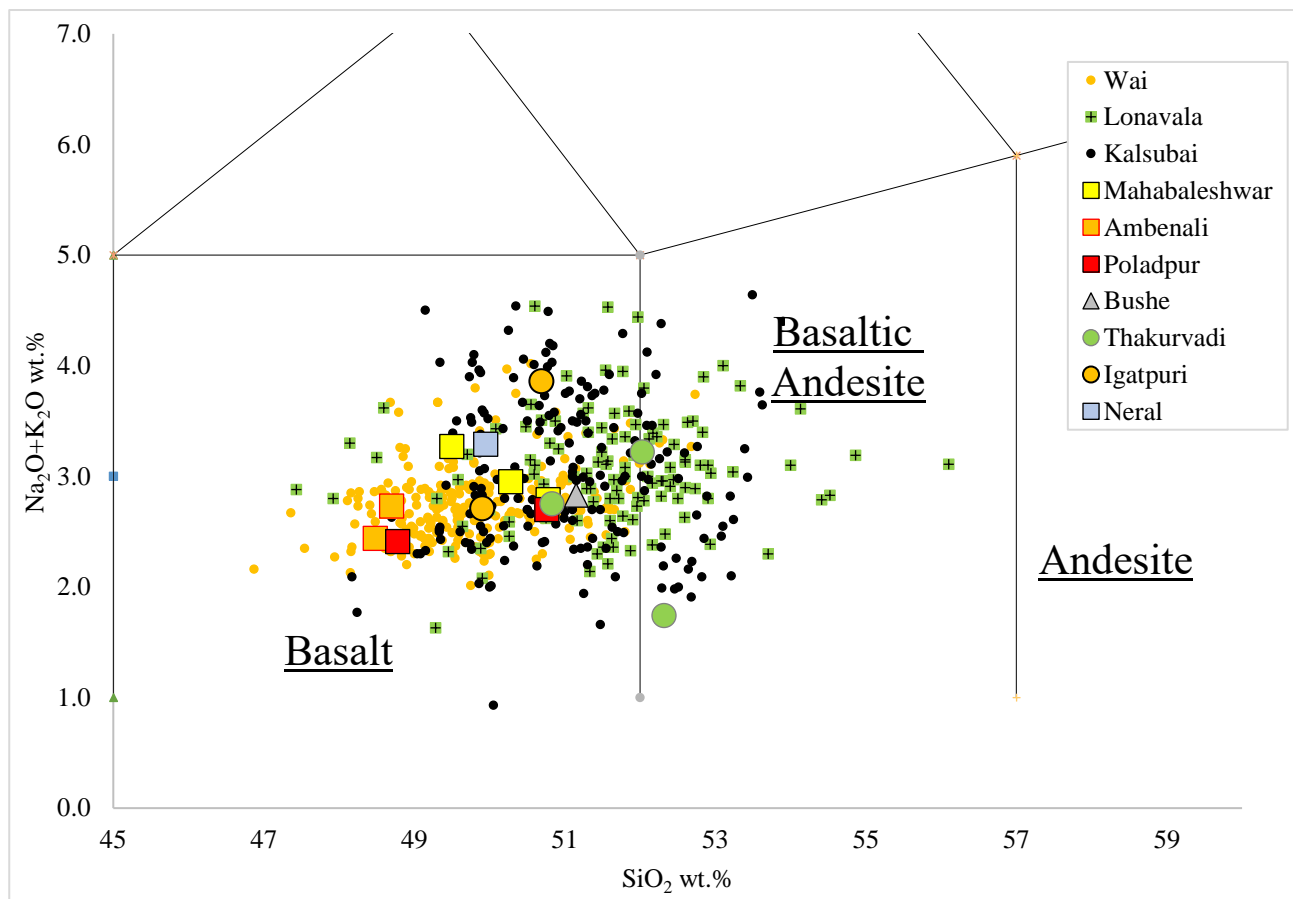
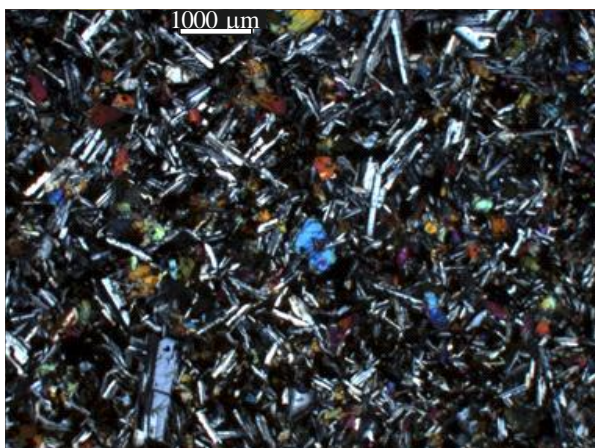
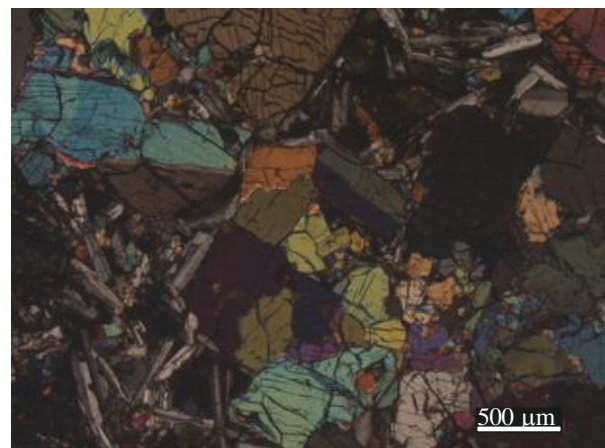


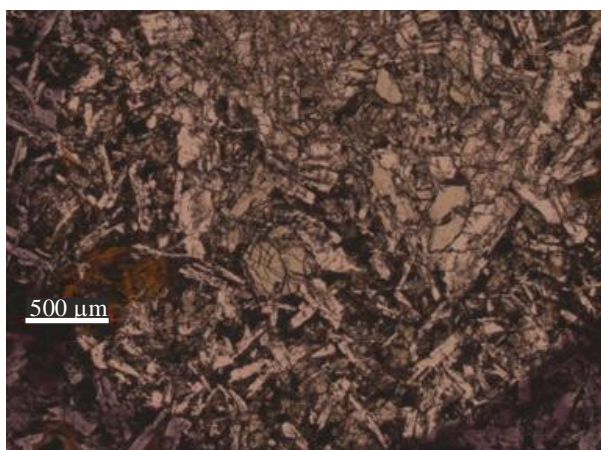
Figure S1: Total alkali silica (TAS) classification diagram (Le Bas et al., 1986). Literature data are from Pakulla et al. (2023) and are shown by small circles (black for Kalsubai, green for Lonavala, and orange for Wai samples).



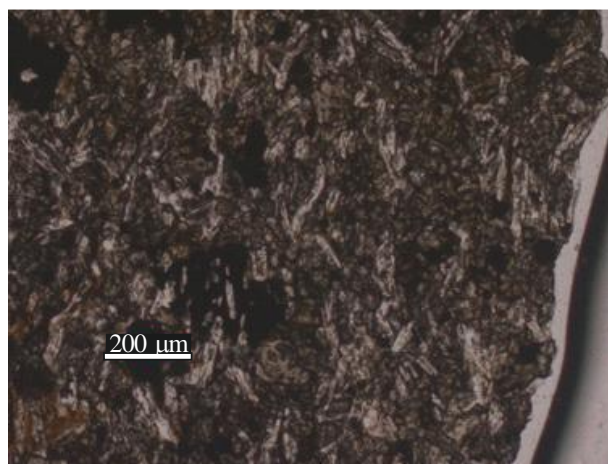
MAT14-2 Neral Fm.



BOR14-2, Thakurvadi Fm.



KAM14-1, Bushe Fm.



AMB14-6, Ambenali Fm.

Figure S2: Thin section microphotographs of representative samples.

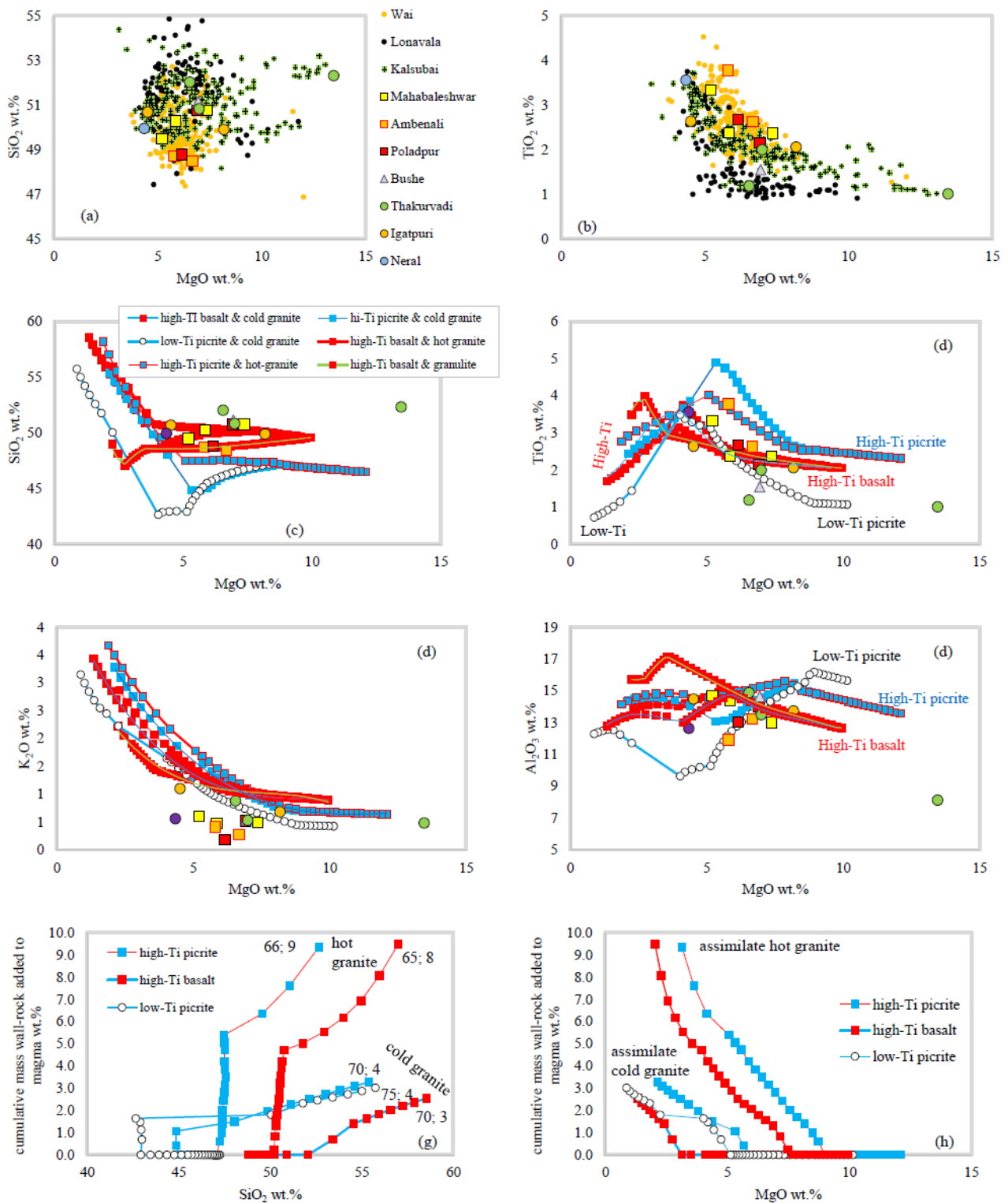


Figure S3: Major element variations (wt.%) for the studied Western Ghats rocks. In panels a and b, literature data (Pakulla et al. 2023, and references therein) are shown by small circles (black for Kalsubai, green for Lonavala, orange for Wai basalts). Panels c, d, e, f report open-system liquid



lines of descent calculated with Magma Chamber Simulator (Bohrson et al., 2020). Starting magma compositions are D44 (a high-Ti picrite from Melluso et al., 2006; calculated liquidus T 1300 °C), JEB15 (a high-Ti basalt from the Kalsubai, Basu et al., 2020; calculated liquidus T 1270 °C), and D56 (a low-Ti picrite, Melluso et al., 2006; calculated liquidus 1260 °C; all parental magma compositions are shown in Table S2). The assimilated crustal rock is a Dharwar Craton granite from Ravindran et al. (2020) with an initial T of 400 or 600 °C (calculated solidus T = 660 °C) and a granulite (Taylor and McLennan, 1985) with an initial T of 650 °C (solidus T 700 °C; whole-rock compositions of the assimilants are in Table S2). Assimilation starts when the magma reaches a T of ca. 1140-1100 °C (ca. 150-200 °C lower than the magma liquidus T) and MgO is ca. 5.9-3.3 wt.%, after ca. 40-55 wt.% fractionation for the magmas assimilating the “cold” granitic and the granulitic crustal rocks, while the assimilation of the “hot” granites starts after ca. 10 wt.% fractionation at T of ca. 1200 °C (ca. 100 °C lower than the magma liquidus T). Graphs g and h show the variations of SiO<sub>2</sub> and MgO of a basalt assimilating a “cold” (400 °C initial temperature) and a “hot” granite (initial temperature 600 °C). For the “cold” granite, more than ca. 2-3 wt.% assimilation drives the contaminated magma to relatively high SiO<sub>2</sub> (> 52 wt.%) and low MgO (< 3 wt.%), i.e., to compositions more evolved than basaltic. By contrast, similar compositions of the contaminated magma would be reached by about 6-8 wt.% assimilation of the hot granite. The numbers next to the last steps at highest SiO<sub>2</sub> in panel g represent the amount of fractionation and of wall-rock assimilation for each case (values in wt.%; note that these values correspond also to the points at lowest MgO plotted in panels c-f, and h). The temperatures corresponding to the highest SiO<sub>2</sub> point in panel g are ca. 1100-1090 °C for the “hot granite” runs, i.e., ca. 200 °C below the magma liquidus temperature, while they are ca. 1060-1080, ca. 230 °C below the magma liquidus temperature.

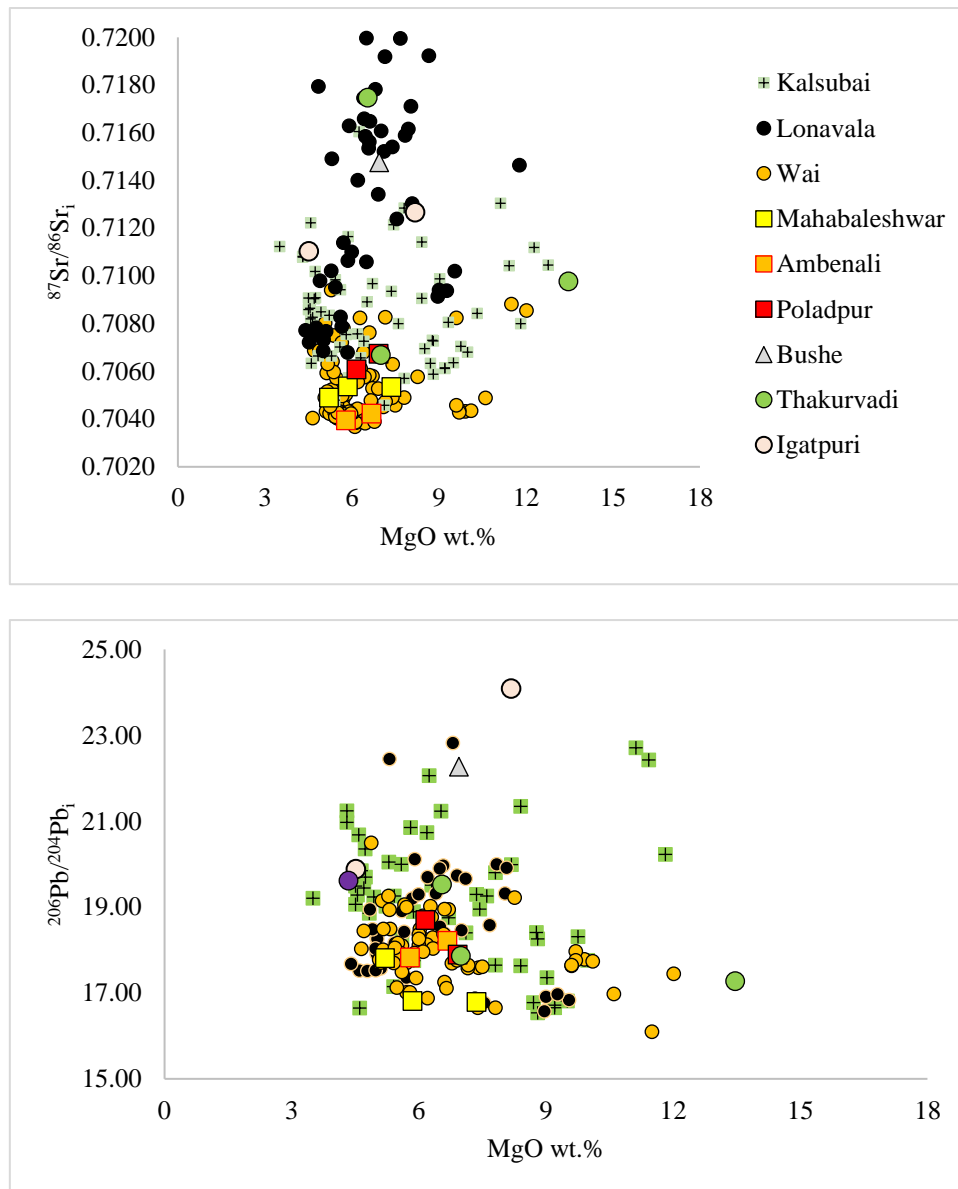


Figure S4: major element (wt.%) vs initial (66 Ma) Sr and Pb isotopic ratios for the studied rocks.

Same symbols and literature sources as in Figure S1.

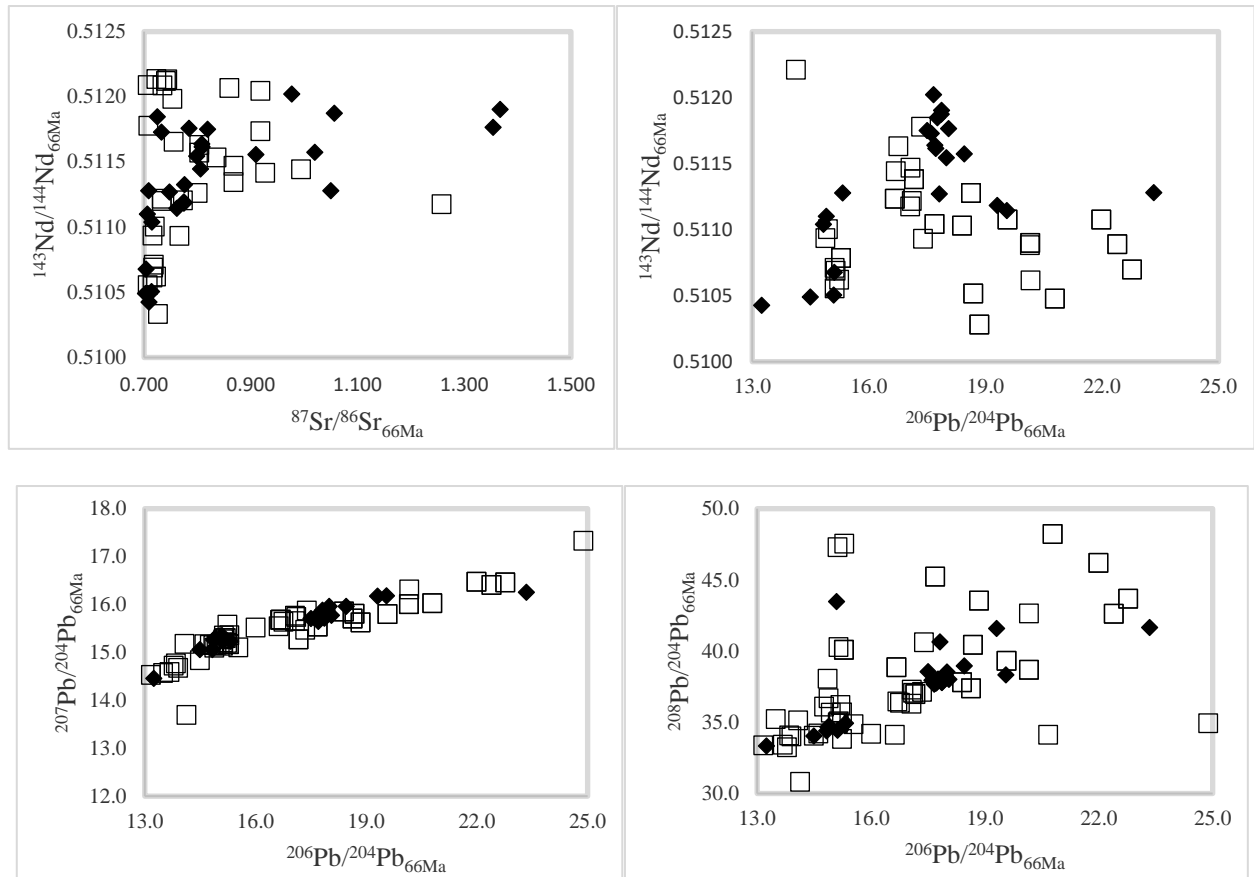


Figure S5: Sr-Nd-Pb isotopic compositions of the Indian basement from the Dharwar craton and the Central Indian Tectonic Zone (compiled from: Alam et al., 2021; Mohan et al., 2013; Peucat et al., 1989; 2013; Ravindra et al. 2020, 2021, 2023; Rickers et al., 2003; Youssouf et al., 2019). All the isotopic compositions were recalculated for an age of 66 Ma. Black diamonds are mafic crustal rocks, white squares are felsic crustal rocks.

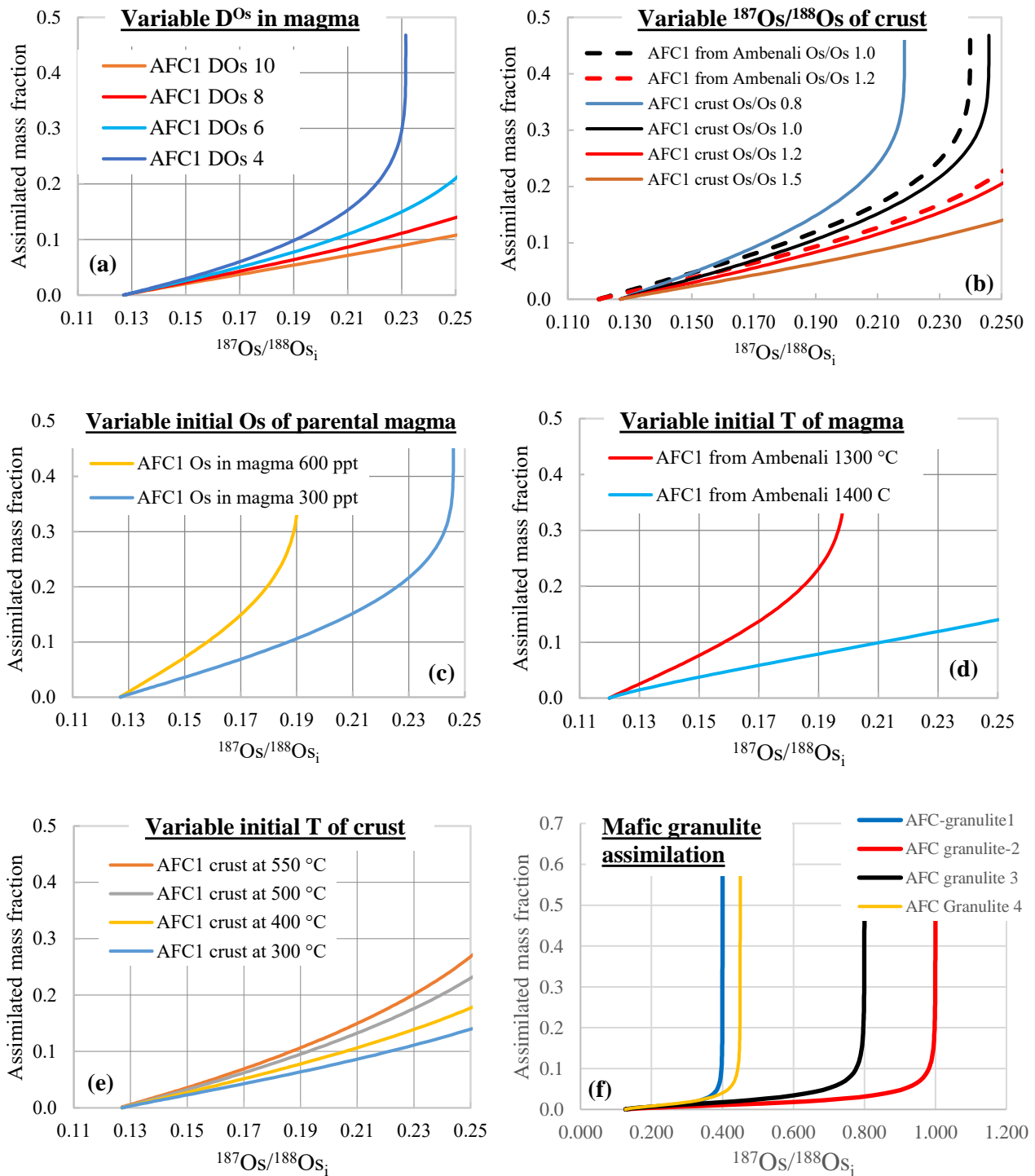


Figure S6:  $^{187}Os/^{188}Os$  vs. assimilated mass fraction, EC-AFC modelling. In a to c, the assimilant is represented by the felsic crust reported in Table S3 (assimilant 1). In all diagrams except in b, the parental magma is the low-Ti picrite with composition reported in Tables S2 and S3. In (b) the parental magma is an Ambenali basalt (dashed lines) or the low-Ti picrite. (a)  $D_{Os}$  are the assumed bulk partition coefficients for Os in the evolving magma. (b) Results for variable isotopic composition of the assimilated crust. The continuous and dashed lines show results starting from a

low-Ti picrite and an Ambenali-like composition, respectively (starting magma compositions in Tables S3). In (c) the initial Os content of the parental magma is considered = 300 and 600 ppt, respectively (for both  $D^{Os} = 8$ ). (d) Shows the EC-AFC results assuming an initial magma T of 1300 and 1400 °C ( $D^{Os} = 8$ ). (e) shows the EC-AFC curves at variable T of the assimilant, ranging from the solidus T (550 °C) to 300 °C ( $D^{Os} = 8$ ).

(f) Shows the EC-AFC curves assuming these 4 granulite compositions: granulite 1, [Os] = 100 ppt,  $^{187}\text{Os}/^{188}\text{Os} = 0.4$  (composition calculated for an age of 2.5 Ga for the granulite with lowest  $^{187}\text{Re}/^{188}\text{Os}$  from Saal et al., 1998); granulite 2, [Os] = 50 ppt,  $^{187}\text{Os}/^{188}\text{Os} = 1$  (composition calculated for an age of 2.5 Ga for the average granulite composition from Saal et al., 1998); granulite 3, [Os] = 30 ppt,  $^{187}\text{Os}/^{188}\text{Os} = 0.9$  (composition calculated for an age of 2 Ga for the for the average granulite composition from Saal et al., 1998); granulite 4, [Os] = 50 ppt,  $^{187}\text{Os}/^{188}\text{Os} = 0.45$  (composition calculated for an age of 1 Ga for the average granulite composition from Saal et al., 1998).

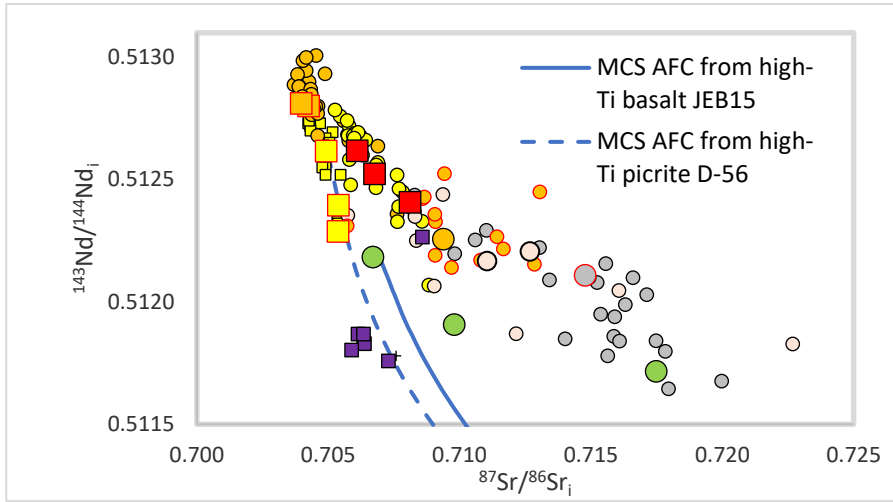


Fig. S7: Magma Chamber Simulator (MCS) modelling of Sr-Nd isotopic variations (initial values at 66 Ma). Starting magmas are a High-Ti picrite (D56 sample, Melluso et al., 2006) and a High-Ti basalt (JEB15 from Basu et al., 2020). The assimilant is equivalent to the low-Sr granite reported in Table S2. The input pressure is 0.2 GPa. The selected near-primitive compositions appear to be possible parental magmas for a few evolved WG basalts for the selected assimilant and physical conditions.

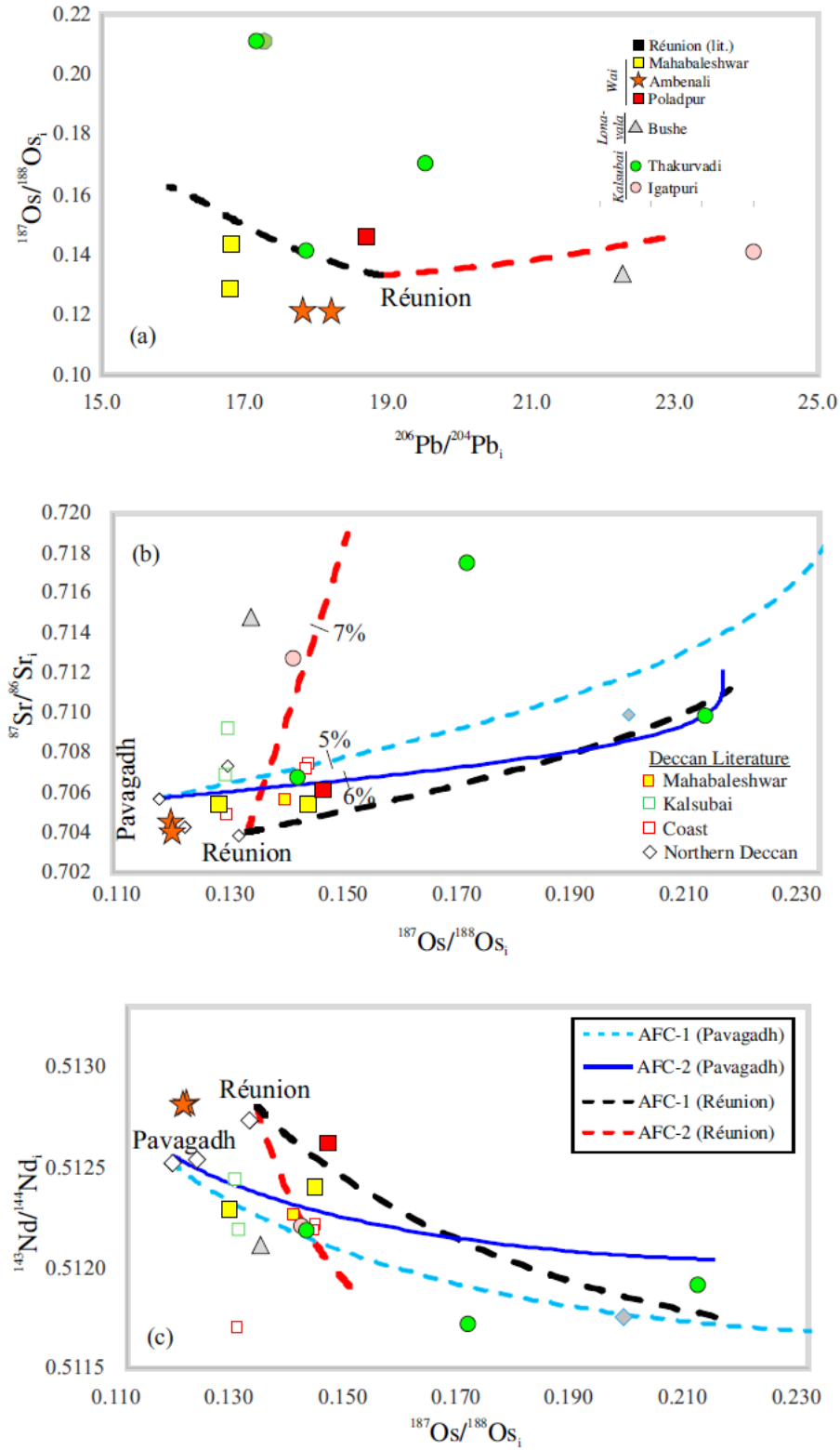


Figure S8: isotopic variations of Deccan basalts and EC-AFC assimilation curves starting from a Réunion and a Mt. Pavagadh (Northern Deccan; Peters et al., 2017) parental magma composition. The assimilated rocks and parental magma compositions are reported in Table S3. Starting from both parental magma compositions, Os isotopic compositions of less than 0.15 for the analyzed WG

basalts require less than 6 wt.% assimilation of the considered crustal rocks. We note that if extremely low (and unlikely values for Proterozoic to Archean basement) Os contents and isotopic compositions are assumed for the assimilated crust (e.g.,  $^{187}\text{Os}/^{188}\text{Os} = 0.8$ ,  $[\text{Os}] = 5$  ppt), the degree of contamination necessary to reach the  $^{187}\text{Os}/^{188}\text{Os}$  of ca. 0.15 would be significantly higher (>20%). However, in order to reproduce the observed Sr-Nd isotopic compositions for such large degrees of assimilation, the contaminant would also need to have significantly lower  $^{87}\text{Sr}/^{86}\text{Sr}$  and higher  $^{143}\text{Nd}/^{144}\text{Nd}$  compared to the typical compositions of Proterozoic and Archean felsic rocks from India (Supplementary Fig. S4).



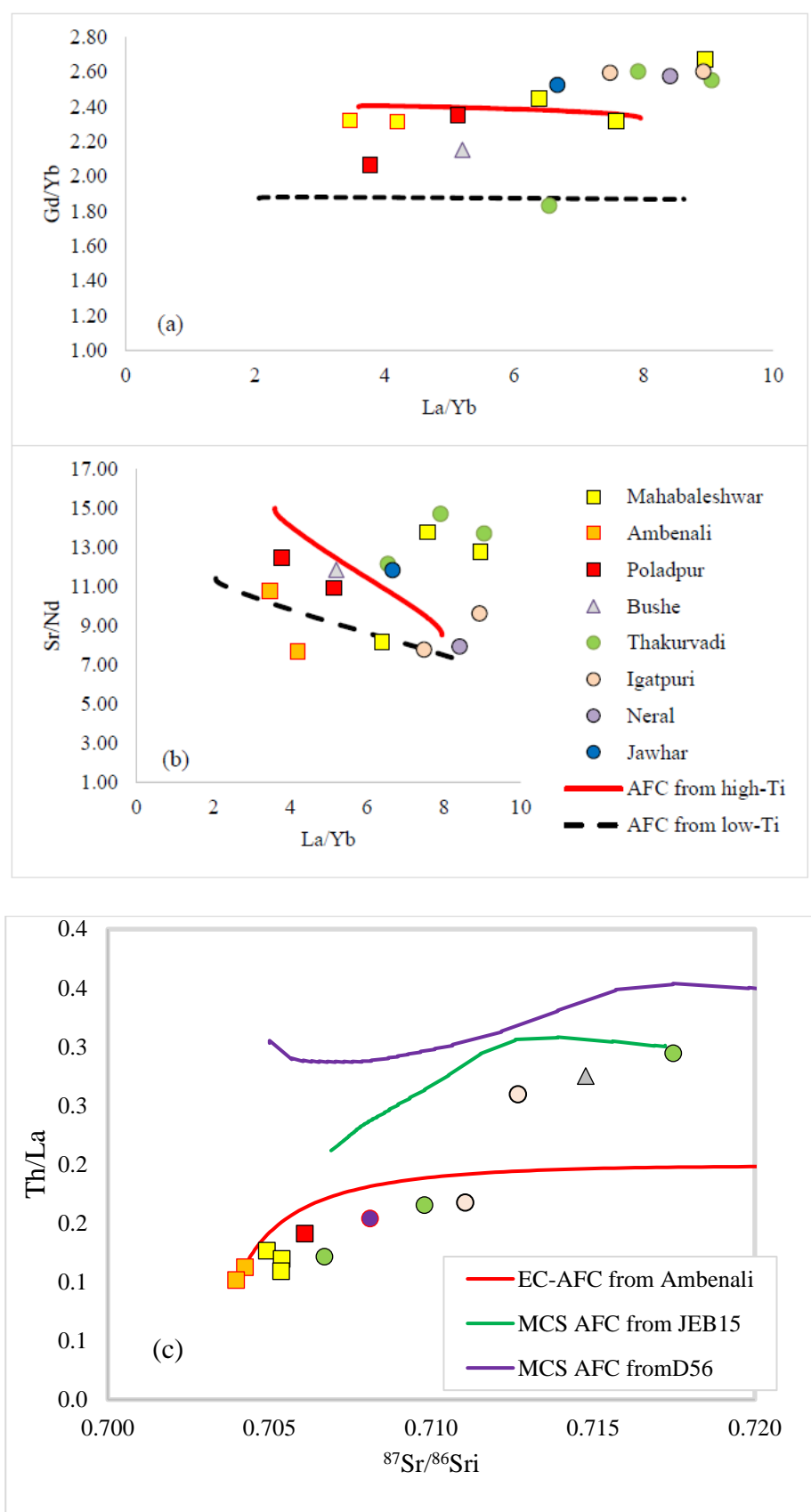


Figure. S9: a and b, trace element ratio variations in studied rocks compared to EC-AFC modelling of assimilation of the felsic assimilant 1 (Table S3) starting from a high- and a low-Ti parental

magma. Panel c shows Th/La vs  $^{87}\text{Sr}/^{86}\text{Sr}_i$  (at 66Ma) compositions modelled with EC-AFC and MCS, considering three distinct parental magmas (Ambenali, high-Ti basalt JEB15 from Basu et al., 2020, and the high-Ti picrite D56 from Melluso et al., 2006; data in Table S3) contaminated by a granitic basement rock.